The approach of a sphere to a wall at finite Reynolds number

A. MONGRUEL[1]†, C. LAMRIBEN[1]‡, S. YAHIAOUI[1] AND F. FEUILLEBOIS[2]

[1]PMMH (CNRS UMR 7636, ESPCI, Université Pierre et Marie Curie-Paris 6 and Université Paris Diderot-Paris 7) 10, rue Vauquelin, 75231 Paris Cedex 05, France

[2]LIMSI-CNRS, UPR 3251, B.P. 133, 91403 Orsay Cedex, France

The approach to a wall of a non-Brownian rigid spherical particle, settling in a viscous fluid with a Reynolds number of the order of unity, is studied experimentally. Far from the wall, the fluid motion around the particle is driven by inertia and viscosity forces. The particle Stokes number is also of the order of unity, so that the particle motion far from the wall is driven by inertia. In the close vicinity of the wall, however, the particle–wall hydrodynamic interaction decelerates the particle significantly. An interferometric device is used to measure the vertical displacement of a millimetric size spherical bead at distances from the wall smaller than 0.1 sphere radius, with a spatial resolution of 100 nm. For the range of impact Stokes number ($St^\star$, based on the limit velocity of the sphere in an unbounded fluid) explored here (up to $St^\star \cong 5$), the measurements reveal that a small region of negligible particle inertia still exists just prior to contact of the sphere with the wall. In this lubrication-like region, the particle velocity decreases linearly with decreasing particle–wall distance and vanishes at contact, ruling out the possibility of a rebound. The vertical extent of this region decreases with increasing Stokes number and is e.g. only 10 μm large at impact Stokes number $St^\star \cong 5$.

Key words: particle/fluid flow

1. Introduction

In a first step towards a comprehensive treatment of suspensions of particles interacting with walls (e.g. of a container), it is useful to consider elementary situations such as a single spherical particle approaching a wall. This paper is limited to the case when the particle and fluid density are of the same order of magnitude, e.g. for solid particles in a liquid. When the Reynolds number of the flow around a particle is low compared with unity, creeping flow equations apply and a single sphere in unbounded fluid settles at the Stokes velocity

$$V_{St} = \frac{2}{9} \frac{(\rho_p - \rho_f) g a^2}{\mu}, \tag{1.1}$$

† Email address for correspondence: anne.mongruel@upmc.fr

‡ Present address: FAST (CNRS UMR 7608, Université Pierre et Marie Curie-Paris 6 and Université Paris-Sud 11) Batiment 502, Campus Universitaire d'Orsay, 91405 Orsay Cedex, France.

where a is the sphere radius, ρ_p is the density of the particle, ρ_f is the fluid density and μ is the fluid viscosity. Here, the associated low Reynolds number is defined as $Re = (2a)\rho_f V_{St}/\mu$. Consider now a particle near a wall, let h be the gap between the particle and wall and let $\varepsilon = h/a$ be the normalized gap. For a spherical particle approaching a wall with a velocity $V_p(\varepsilon)$, for instance when settling under gravity, the drag force F_D may be written as $F_D = 6\pi\mu a V_p(\varepsilon) f_{zz}(\varepsilon)$, where the dimensionless friction factor $f_{zz}(\varepsilon)$ is a function of the normalized gap ε. This friction factor was calculated theoretically as a series (see Brenner 1961; Maude 1961) using the technique of bi-spherical coordinates. This exact solution was verified experimentally (see Ambari, Gauthier-Manuel & Guyon 1984; Lecoq et al. 1993). In the lubrication region, i.e. when the particle–wall distance is smaller than roughly 0.01 sphere radius, the exact solution by Maude (1961) and Brenner (1961) coincides within a 1 % error with the standard approximate lubrication theory (see e.g. Cox & Brenner 1967): $f_{zz}(\varepsilon) = 1/\varepsilon$. It also coincides within 1 % error for $\varepsilon < 0.25$ with the three terms asymptotic expansion for small gap ε of Cox & Brenner (1967)

$$f_{zz}(\varepsilon) = \frac{1}{\varepsilon} + \frac{1}{5}\ln\left[\frac{1}{\varepsilon}\right] + 0.9713. \qquad (1.2)$$

Note that the second (ln) term in the asymptotic expansion, if taken alone, does not improve over the first term, since it is practically of the same order as the third term (unless ε is very small, which is not practically useful here). Since fluid inertia is negligible and fluid and particle density are of the same order, particle inertia is also negligible and the balance of forces on the moving sphere gives $V_p(\varepsilon) f_{zz}(\varepsilon) = V_{St}$ during the whole motion of the sphere. Hence, keeping only the first term in (1.2), in the lubrication region ($\varepsilon \ll 1$) and for negligible fluid inertia ($Re \ll 1$), $V_p(\varepsilon) = V_{St}\,\varepsilon$: the particle velocity decreases linearly in ε as the particle approaches the wall, the slope of the velocity versus dimensionless gap curve being the Stokes velocity. A lubrication drag force that is inversely proportional to the separation distance thus leads to the well-known paradox that the sphere would only asymptotically make contact with the wall. However, in practice, this theory breaks down for various reasons, among them the roughness of the real surfaces allowing contact in a finite time (see Smart & Leighton 1989; Lecoq et al. 2004). Yet, resolving the question of a possible collision of a particle on a smooth wall remains a challenge. It is clear that fluid inertia may participate in this question.

Small effects of fluid inertia in the lubrication region were calculated by Cox & Brenner (1967) using the method of matched asymptotic expansions, with the following result:

$$f_{zz}(\varepsilon, Re) = \frac{1}{\varepsilon} + \frac{1}{5}\left[1 + \frac{Re}{4}\right]\ln\left[\frac{1}{\varepsilon}\right] + O(Re^2), \qquad (1.3)$$

valid for $\varepsilon \ll 1$ and $\varepsilon Re \ll 1$. Note that here the sphere is moving towards the wall with a constant velocity. In this problem, the fluid flow is geometrically unsteady; this has been taken into account in this formula. Unfortunately, for $Re \to 0$, formula (1.3) does not provide a good approximation to $f_{zz}(\varepsilon)$ without the next-order (constant) term appearing in (1.2), unless ε is very small, as explained after (1.2). It is not known at this stage whether the constant term 0.9713 could simply be added in (1.3) since the $O(Re^2)$ term has not been calculated. Nevertheless, formula (1.3) is useful in providing the following estimate. For small values of Re and ε, the second-order correction (ln) term appears to be quite small compared to the leading order one, which is the standard lubrication friction coefficient. As a consequence, according to

this formula, the effects on the drag force of a small fluid inertia would be rather difficult to detect experimentally. In order to resolve experimentally the influence of fluid inertia, we thus consider cases where the Reynolds number is of order unity.

At $Re \cong 1$, a variety of situations may occur depending on whether the inertia of the particle approaching the wall is sufficient, or not, to make it collide with the wall. Particle inertia is usually quantified by a Stokes number, defined as the ratio of particle inertia to viscous forces. The problem of a sphere approaching a wall is unsteady, so that the velocity and Reynolds number based on this velocity depend on the distance to the wall. Taking V_{St} as a characteristic velocity for the particle, we thus define a particle Stokes number $St = m_p V_{St}/6\pi\mu a^2 = ((\rho_p/\rho_f)/9)Re$, where m_p is the mass of the particle. With fluid and particle densities having the same order of magnitude, the particle Stokes number is of the same order as the Reynolds number based on the Stokes velocity. Earlier studies have dealt with the collision of the particle with the wall in this configuration, focusing attention on the critical value of Stokes number above which the particle is able to rebound off the wall (Davis, Seyrassol & Hinch 1986; Barnocky & Davis 1988). In the study by Gondret *et al.* (1999), the whole trajectory of a sphere fully immersed in a fluid is recorded during its approach of the wall, and the transition from the non-bouncing to the bouncing regime is found at a critical Stokes number $St^\star \cong 20$. Note that here, $St^\star$ is an impact Stokes number, based on the impact velocity (limiting velocity far from the wall). Later studies (Joseph *et al.* 2001; Gondret, Lance & Petit 2002) showed that this transition is more precisely situated at $St^\star \cong 10$. Further studies are needed for detailing how near-wall hydrodynamic interactions may slow down the particle to such an extent as to hinder collision.

To summarize, this study is concerned with a spherical non-Brownian particle settling by gravity towards a horizontal plane wall, in the case where the fluid has a finite inertia far from the wall ($Re \cong 1$), and the fluid and particle densities are of the same order of magnitude. Hence, the particle enters the near-wall region ($\varepsilon < 0.1$) with a non-negligible inertia. The focus of this experimental study is the particle dynamics in this region ($\varepsilon < 0.1$). Values of particle Stokes numbers, based on the Stokes velocity, are in the range $0.6 \leqslant St \leqslant 9.2$, and are, therefore, limited to the non-bouncing regime. The experimental set-up and results are presented in §2. In §3, a simple semi-empirical model is presented and compared to experimental results. Finally, the conclusion is in §4.

2. Experiments

The displacement of a sphere of millimetric size is measured with an interferometric device, with a resolution on the displacement of 100 nm. This technique provides minute accuracy for the sphere displacement in this near wall region. The device, which is used here, was already described by Lecoq *et al.* (1993). The settling sphere is used as a reflector in the interferometer, and its displacement makes the interference fringe pattern (circular rings) move accordingly. The recorded signal is the light intensity at the centre of the interference pattern. As a consequence, a signal variation from a maximum (bright fringe) to another maximum (bright fringe) is due to a displacement of the sphere equal to $\lambda/4n$, where λ is the wavelength of the laser, and n is the index of refraction of the suspending fluid. Here, with an He–Ne laser beam ($\lambda = 632.8$ nm) and a silicon oil ($n = 1.404$), we have $\lambda/4n = 112$ nm. The velocity v_p of the sphere is related to the velocity of fringe displacement by $v_p = (\lambda/4n)/\Delta t_m$, where Δt_m is the elapsed time between two maxima of the signal. Thus, the spatial

resolution of the device depends on the frequency of the data acquisition system. If this acquisition system is able to detect the extrema of the signal, it provides an accuracy on the displacement of the sphere of the order of $0.06\,\mu m$, which is better than most standard visualization techniques, and also quite small compared with the particle size, the ratio being at most $\Delta\varepsilon = 10^{-5}$ corresponding to the smallest sphere that we use ($2a = 5.55\,mm$).

Originally (see Lecoq *et al.* 1993), this interferometric device was designed to follow the motion of a sphere at $Re \cong 10^{-5}$. Here, an improved data acquisition system has been developed for following faster motions of the sphere up to around $100\,mm\,s^{-1}$. At this velocity, the signal frequency is $1/\Delta t_m \cong 0.9\,MHz$. The data acquisition then should have a frequency at least 10 times larger, i.e. $10\,MHz$. The opto-electronic conversion is made via a photo-multiplier tube (R1894 from Hamamatsu) whose response time of $0.8\,ns$ is much smaller than the data acquisition period. Its quantum efficiency at $\lambda = 632.8\,nm$ is sufficiently large. At the output of the photo-multiplier tube the electric-signal intensity is low, so that it is necessary to adapt the impedance and amplify the signal. This is done via a tailored operational amplifier device with bandwidth $4.2\,Hz - 1.2\,MHz$, that ensures the amplification in a frequency range of two orders of magnitude larger than the one in the earlier set-up. The signal is recorded with a high-frequency electronic oscilloscope (DPO4032 from Tektronics) whose maximal memory length is fixed to 1M points. The recorded signal is transferred to a PC and processed by a Matlab code for extracting the extreme values of the signal as a function of time. The key point of the algorithm is a detection of the extrema that is not affected by the noise. It applies a 'backwards following up' (step by step) method, starting from the arrival of the sphere at the plane wall. In practice, the robustness of this procedure has been proven in a range where the ratio of a given frequency to the next one is smaller than 1.5. For the highest frequency, for which they were only around 10 points per period, the noise increased and the frequency was averaged over 7–8 periods (75 points).

The sphere is embedded in a fluid contained in a cylindrical vessel with a $80\,mm$ diameter and a $40\,mm$ height. The lateral walls are made with altuglass, and the top and bottom plane walls are made of glass of optical quality. The vessel is filled up with a PDMS (polydimethylsiloxane or silicone) oil (either 47V1000 or 47V12500 Rhodorsyl oil, manufactured by Rhone–Poulenc), with density of $\rho_f = 978\,kg\,m^{-3}$ and kinematic viscosities 12.5×10^{-3} and $10^{-3}\,m^2\,s^{-1}$, respectively at $25\,°C$. The air-conditioned room temperature was $23\,°C$. Physical properties of the oil (viscosity, refraction index) vary slowly with temperature. The oils have a Newtonian behaviour for shear rates up to 2000 and $200\,s^{-1}$, respectively. The particles are spherical steel balls with density $\rho_p = 7.8 \times 10^3\,kg\,m^{-3}$ and with diameters ranging from 5.55 to $14\,mm$. At the beginning of the experiment, the sphere is held at the centre of the top plane window with a magnet. It is then released by rapidly taking away the magnet. This creates small initial perturbations that may cause the trajectory of the sphere not to be aligned with the vertical laser beam. The subsequent motion of the sphere lasts only a few tenths of a second, so that it is not possible to manually readjust the position of the laser beam during this motion. Therefore, experiments have to be repeated several times until a vertical trajectory is obtained in the vicinity of the wall. The contact position with the bottom wall is defined from the recorded signal, when the period of the signal becomes very large indicating a vanishing velocity (see figure 1*a*). Then, the error on contact position is around $\lambda/4n = 112\,nm$. This contact fixes the zero value for the vertical axis and the preceding positions of the sphere are reconstructed from it using the calculated velocity for each signal period.

Diameter 2a (mm)	Calculated values			Measured values				Critical distance		
	V_{St} (m s^{-1})	Re	St	V_{St}^m (m s^{-1})	$\Delta V_{St}^m / V_{St}^m$	V_{St}^m / V_{St}	St_m	h_c (mm)	ε_c	$\varepsilon_c St_m$
5.55	0.12	0.65	0.58	0.12	0.002	1.04	0.63	0.150	0.0541	0.034
6.35	0.15	0.97	0.85	0.16	0.001	1.07	0.99	0.125	0.0394	0.039
8.00	0.24	1.95	1.72	0.28	0.001	1.14	2.25	0.080	0.0200	0.045
10.5	0.42	4.40	3.90	0.51	0.003	1.20	5.66	0.040	0.0076	0.043
12.7	0.61	7.79	6.90	0.77	0.035	1.26	10.91	0.0172	0.0020	0.034
14.0	0.75	10.43	9.24	0.98	0.035	1.31	15.96	0.0094	0.0013	0.021

TABLE 1. Data for spheres (steel balls) of different diameters settling in 47V1000 silicon oil.
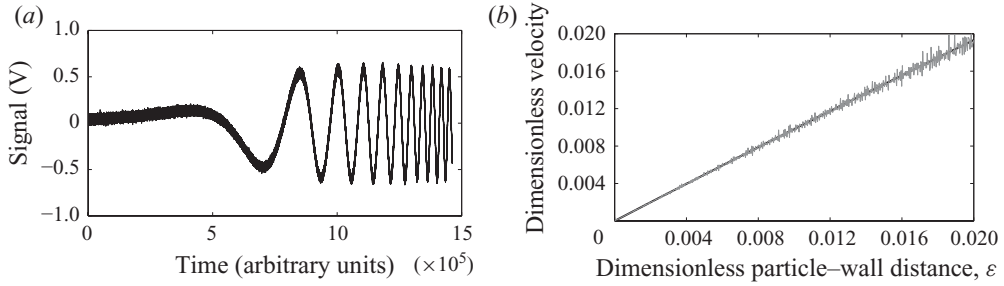

FIGURE 1. Experiments at small Reynolds number (sphere of 12.7 mm diameter settling in 47V12500 silicone oil towards a glass wall). (*a*) Example of raw signal recorded as a function of time (the sphere approaches close to the wall from right to left and eventually stops). (*b*) Normalized velocity versus normalized gap in the lubrication region (scattered line: experiments, straight line: linear regression).

Typical results obtained in the conditions of a small Reynolds number are shown in figure 1 (sphere of 12.7 mm diameter in V12500 silicone oil, $Re = 2.3 \times 10^{-2}$). Here a data acquisition frequency of 2.5 MHz was used. Figure 1(*a*) depicts the signal evolution for a sphere arriving at the plane wall, showing the increasing period of the signal until contact occurs. Note that the signal-to-noise ratio deteriorates at vanishing frequency, because the low frequency limit of the oscilloscope is reached. Figure 1(*b*) is a zoom on the lubrication region, showing the linear variation of the measured dimensionless velocity, V_p / V_{St}^m, with dimensionless distance ε, where the measured characteristic velocity, V_{St}^m, is determined from a linear regression. Here, no filter has been applied on the measured frequency in the lubrication region. We find $V_{St}^m = 49.35$ mm s^{-1}, in perfect agreement with the expected value from Stokes formula (1.1). The maximum velocity in the cell corresponds to a signal frequency of $\cong 0.3$ MHz that would not have been detected by the original device.

Measurements of the particle velocity in the lubrication region at $Re \cong 1$ and $St \cong 1$ were performed using the 47V1000 silicone oil, and steel balls of different diameters ranging from 5.55 to 14 mm. Values of the characteristic velocity V_{St}, calculated from Stokes formula, and the Reynolds and Stokes numbers based on this velocity, are shown in table 1. The range of Reynolds numbers is between 0.65 and 10.4. As the sphere diameter increases, the settling velocity increases as well and the range of experimentally accessible particle–wall gaps reduces, as a consequence of the velocity being closer to the upper cutoff of 100 mm s^{-1}. Then we focus on a region smaller than 0.35 mm close to the wall where the velocity stays small enough. The results for
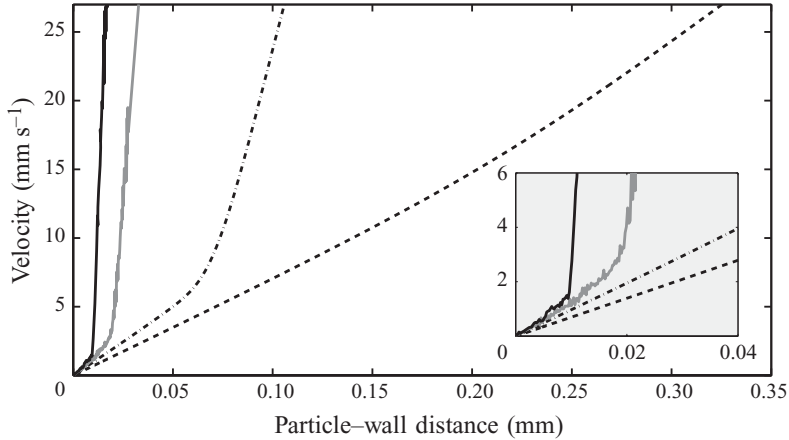
FIGURE 2. Experiments at finite Reynolds number (steel balls of different diameters falling in 47V1000 silicone oil towards a glass wall): velocities of settling spheres with diameter 8, 10.5, 12.7 and 14 mm, as a function of the sphere-to-wall distance. The diameter of the spheres increases from right to left. Insert: zoom on the close vicinity of the wall.

the measured particle velocity as a function of the particle–wall distance are shown in figure 2. For particles with the largest diameters, the measurements exhibit a clear transition between a nonlinear evolution of the velocity far from the wall and a linear one close to it. As the Reynolds number increases, the spatial extent of the linear region is reduced, as shown by the zoom in that region (see insert of figure 2). From each experimental curve, we have extracted the distance to the wall, h_c, at which the linear regime ends, i.e. at which the velocity is greater than the one expected by extrapolating the linear variation. (Note that the change from one regime to the other is better defined as the Reynolds number increases.) The values of h_c are reported in table 1, together with their dimensionless form $\varepsilon_c = h_c/a$. We stress that for the largest sphere used in these experiments, there still exists a linear region for the velocity–distance curve just prior to contact, within a distance of $h_c \cong 10\,\mu m$ from the wall. This region could be hardly studied with a video device. Our measurements thus complement those by Gondret *et al.* (1999) who used visualization with a high-speed video camera, whose precision on the particle position (4 % of particle radius) was not sufficient in the lubrication region. For a direct comparison with their experiments, we need an impact Stokes number, $St^\star$, based on the limit velocity of a sphere in an unbounded fluid at $Re = O(1)$. This limit velocity may be estimated in our experiments, neglecting the effects of sidewalls, by solving the steady motion of the sphere, and using Oseen's formula for the friction factor ($f_{zz} = 1 + 3Re/16$; Happel & Brenner 1983). For our largest sphere, we find that the impact Stokes number is $St^\star \cong 5$. This is lower by a factor of about 2 than the critical impact Stokes number for bouncing transition (Gondret *et al.* 2002).

3. Discussion

The results for the slope of the linear part of the velocity–distance curve, V_{St}^m, are displayed in table 1 together with the relative precision $(\Delta V_{St}^m)/V_{St}^m$ (their repeatability corresponds to a range of four measurements). Note that, as the Reynolds number increases, the linear regression is calculated on a smaller region, with more scattered data, so that the precision deteriorates. This characteristic velocity V_{St}^m is found to be systematically larger than the Stokes velocity, V_{St}, that would be expected from (1.1),

with a relative difference that increases with Re, being only 4.2 % at $Re = 0.65$, but reaching 31.4 % at $Re = 10.4$. Several factors may be invoked to interpret measured values of V_{St}^m that are larger than expected. Non-Newtonian effects are negligible. Temperature effects or pre-shear effects due to repeated tests on the same oil within a few minutes are ruled out. Then, the main effect to be added is due to inertia, as expected for a Reynolds number Re of order unity. Our experiments show a decrease in the friction factor $f_{zz}(\varepsilon, Re)$ with increasing Re and for a given ε. In contrast to our results, (1.3) predicts a friction factor that increases with increasing Re, but, as already mentioned, it is applicable to a sphere moving with a constant velocity towards the wall, which is not the case in our experiments.

We now propose a semi-empirical model for the near-wall region ($\varepsilon \ll 1$), assuming that the whole effect of fluid inertia is included in the friction factor $f_{zz}(\varepsilon, Re)$. Note that the notion of added mass is irrelevant for Reynolds numbers $Re = O(1)$, except for times which are small compared with the time of diffusion of vorticity, which is not the case here. Unsteady inertial terms involving viscosity effects might be more complicated. In this simple model, we ignore any unsteady term that might be due to fluid inertia in this regime $Re = O(1)$. Then the equation of motion is, with $V_p > 0$ pointing down:

$$m_p \frac{\mathrm{d}V_p}{\mathrm{d}t} = -6\pi a\mu V_p \, f_{zz}(\varepsilon, Re) + \frac{4}{3}\pi a^3 (\rho_p - \rho)g. \qquad (3.1)$$

In the region very close to the wall, experiments show that the velocity grows linearly with the normalized gap ε, in the form

$$V_p = V_{St}^m \, \varepsilon, \qquad (3.2)$$

where V_{St}^m is some characteristic velocity. By comparison with (3.1), keeping only the terms on the right-hand side (i.e. neglecting particle inertia), it follows that we take in this region:

$$f_{zz}(\varepsilon, Re) = \frac{1}{\varepsilon} \frac{V_{St}}{V_{St}^m}, \qquad (3.3)$$

where V_{St} is the Stokes velocity. In the particular case $Re \ll 1$, then $f_{zz}(\varepsilon, Re) = 1/\varepsilon$ from the classical lubrication theory and $V_{St} = V_{St}^m$. The fact that a lubrication region exists for very small gaps, even with some fluid inertia, could be expected from (1.3) for small Re. However, (1.3) apparently does not apply to unsteady sphere velocity and Re of order unity, since the experimental friction factor is different from $1/\varepsilon$.

From (3.2), it appears appropriate to use V_{St}^m as a velocity scale. We then define a dimensionless time $\tau = t \, V_{St}^m / a$. Then, $V_p / V_{St}^m = -\mathrm{d}\varepsilon / \mathrm{d}\tau$. We further assume that the friction factor (3.3) can be used in the whole near-wall region ($\varepsilon \ll 1$). Equation (3.1) is then rewritten in dimensionless form as

$$-St_m \frac{\mathrm{d}^2\varepsilon}{\mathrm{d}\tau^2} = \frac{1}{\varepsilon} \frac{\mathrm{d}\varepsilon}{\mathrm{d}\tau} + 1, \qquad (3.4)$$

where St_m is a modified Stokes number, based on V_{St}^m:

$$St_m = \frac{\rho_p \left[V_{St}^m\right]^2}{(\rho_p - \rho_f)ga}. \qquad (3.5)$$

Values of the Stokes number, which is representative of particle inertia in the $Re = O(1)$ regime, are listed in table 1.

Now, for $\varepsilon \ll 1$, but outside of the linear region close to the wall, the inertia term on the left-hand side in (3.1) is large compared with the gravity (weight and
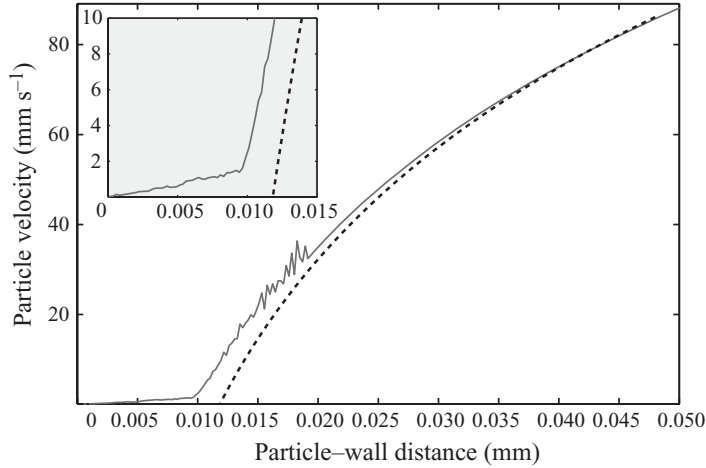
FIGURE 3. Velocity of the sphere as a function of sphere-to-wall distance. Solid line: experiment for a 14 mm diameter steel ball settling in 47V1000 silicone oil towards a glass wall. Dotted line: model neglecting gravity forces, (3.6), with $St_m = 16.0$, $V_{St}^m = 980$ mm s^{-1}, $V_0 = 86.11$ mm s^{-1} and $h_0 = 0.048$ mm. Insert: zoom on the close vicinity of the wall.

buoyancy) term in the right-hand side. Keeping then the first two terms and integrating yields

$$\frac{V_p}{V_{St}^m} = \frac{V_0}{V_{St}^m} + \frac{1}{St_m} \ln \frac{\varepsilon}{\varepsilon_0}, \qquad (3.6)$$

where V_0 is a value of V_p measured at a value ε_0 of the normalized gap ε. Note that a similar result was obtained by Davis *et al.* (1986) in the context of elasto-hydrodynamic collision.

Equation (3.6) reflects the strong deceleration of the sphere under the action of the lubrication drag force. As it further approaches the wall, particle inertia keeps decreasing, until it is sufficiently small so that the dominant terms in (3.1) become in turn the lubrication drag force and gravity forces, yielding (3.2). From (3.4), inertia is negligible compared with gravity at a sufficiently small distance ε_c such that

$$\varepsilon_c \, St_m \ll 1. \qquad (3.7)$$

The crossover between the two velocity regimes is, therefore, controlled by the modified Stokes number, as it is situated at a critical particle–wall distance ε_c that varies like $1/St_m$. We have calculated $\varepsilon_c \, St_m$ for each set of experiment, and found values that are on average equal to 0.036 (see table 1), in agreement with the order of magnitude criteria of (3.7). With increasing Stokes number, the extent of the linear regime reduces, until ε_c becomes comparable to the gap where contact between particle and wall occurs, a distance that is of the order of the height of the roughness of the surfaces coming into contact. It may happen that, following contact, bouncing then occurs. However, this is beyond the scope of this study (see Gondret *et al.* 2002). It may only be remarked that the present simple model would predict a rebound transition independent of gravity, which is consistent with the fact that Joseph *et al.* (2001) and Gondret *et al.* (2002) find similar results for the bouncing transition, regardless of gravity.

To our knowledge, the linear regime at particle Stokes numbers of order unity has not been mentioned elsewhere. In the lack of awareness of the existence of the linear regime, (3.6) would overestimate the particle–wall distance at which the particle velocity vanishes. This is illustrated in figure 3, in which the experimental velocity in
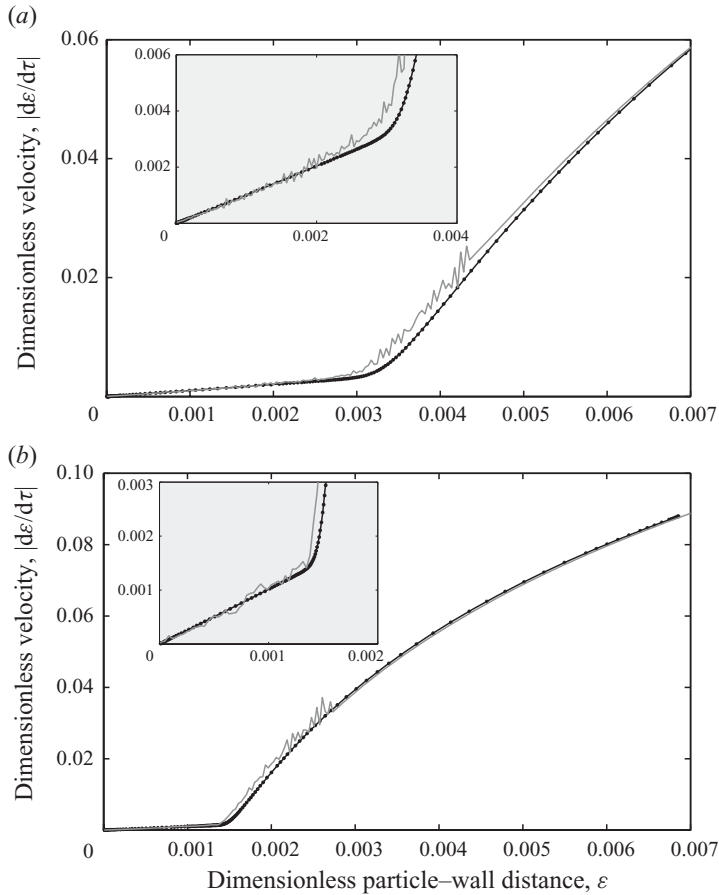
FIGURE 4. Normalized velocity of the settling sphere (normalized by V_{St}^m) as a function of the normalized sphere-to-wall distance. Solid line: experiments for steel balls of diameter (a) 12.7 mm and (b) 14 mm, falling in 47V1000 silicone oil towards a glass wall. Dotted line: numerical model, (3.4), with (a) $St_m = 10.9$ and (b) $St_m = 16$. Insert: zoom on the close vicinity of the wall.

the lubrication region is plotted together with (3.6), taking as initial condition V_0, a measured velocity at a distance h_0. The experimental curve and the model are close far from the wall, starting from the specified initial conditions, but diverge at the transition with the linear regime, leading to a zero velocity at a distance that is rather too far from the wall.

Finally, we have solved numerically the equation of motion of the particle, (3.4), using a predictor–corrector scheme particularly suited for a stiff problem. The initial conditions are experimental ones ($-\mathrm{d}\varepsilon/\mathrm{d}\tau = V_0/V_{St}^m$ at $\varepsilon = \varepsilon_0$), chosen within the lubrication region. The program is stopped at a sufficiently long time for the corresponding calculated value of ε to be close to zero. The results of the simulations are depicted in figure 4, together with the experimental velocity. The agreement between the model and the experiments in the linear regime is the consequence of using V_{St}^m as velocity scale in (3.4). More interestingly, the numerical simulation describes correctly the transition between the two regimes. For instance, the discrepancy between the measured and simulated value of h_c is only 1 μm as shown in figure 4(a). This small discrepancy may be attributed to some unsteady-inertial-viscous drag, the form

of which is presently unknown in the present configuration, to our knowledge. The results show that the scaling by V_{St}^m may be safely extrapolated to the nonlinear regime with correct results. Here the key point is that this semi-empirical model captures the existence of the linear regime in the range of parameters considered here.

4. Conclusion

Measurements of the velocity of a spherical particle approaching a wall with small but non-negligible inertia (impact Stokes numbers of order unity), focusing on the near-wall region (dimensionless particle–wall distances < 0.1), have been proven possible using an interferometric device with high spatial resolution, coupled with a high-frequency data-acquisition system. The resolution of the device reveals two distinct regimes for the dynamics of the particle as the particle–wall distance decreases: first, a nonlinear regime of rapid deceleration, followed by a linear (lubrication-like) regime just prior to contact. The spatial extent of the linear regime decreases with increasing impact Stokes number, but is still detectable in the range of parameters studied here, i.e. to $St^\star \cong 5$.

REFERENCES

AMBARI, A., GAUTHIER-MANUEL, B. & GUYON, E. 1984 Wall effects on a sphere translating at constant velocity. *J. Fluid Mech.* **149**, 235–253.

BARNOCKY, G. & DAVIS, R. 1988 Elastohydrodynamic collision and rebound of spheres: experimental verification. *Phys. Fluids* **31** (6), 1324–1329.

BRENNER, H. 1961 The slow motion of a sphere through a viscous fluid towards a plane surface. *Chem. Engng Sci.* **16**, 242–251.

COX, R. & BRENNER, H. 1967 The slow motion of a sphere through a viscous fluid towards a plane surface. Part II. Small gaps widths, including inertial effects. *Chem. Engng Sci.* **22**, 1753–1777.

DAVIS, R., SEYRASSOL, J. & HINCH, E. 1986 The elastohydrodynamic collision of two spheres. *J. Fluid Mech.* **163**, 479–497.

GONDRET, P., HALLOUIN, E., LANCE, M. & PETIT, L. 1999 Experiments on the motion of a solid sphere toward a wall: from viscous dissipation to elastohydrodynamic bouncing. *Phys. Fluids* **11** (9), 2803–2805.

GONDRET, P., LANCE, M. & PETIT, L. 2002 Bouncing motion of spherical particles in fluids. *Phys. fluids* **14** (2), 643–652.

HAPPEL, J. & BRENNER, H. 1983 *Low Reynolds Number Hydrodynamics*. Kluwer.

JOSEPH, G., ZENIT, R., HUNT, M. & ROSENWINKEL, A. 2001 Particle-wall collisions in a viscous fluid. *J. Fluid Mech.* **433**, 329–346.

LECOQ, N., ANTHORE, R., CICHOCKI, B., SZYMCZAK, P. & FEUILLEBOIS, F. 2004 Drag force on a sphere moving towards a corrugated wall. *J. Fluid Mech.* **513**, 247–264.

LECOQ, N., FEUILLEBOIS, F., ANTHORE, N., ANTHORE, R., BOSTEL, F. & PETIPAS, C. 1993 Precise measurement of particle-wall interactions at low Reynolds number using laser interferometry. *Phys. Fluids* A **5**, 3–12.

MAUDE, A. D. 1961 End effects in a falling-sphere viscometer. *Br. J. Appl. Phys.* **12**, 293–295.

SMART, J. & LEIGHTON, D. 1989 Measurement of the hydrodynamic surface roughness of noncolloidal spheres. *Phys. Fluids* A **1**, 52–60.